JCTC Journal of Chemical Theory and Computation

Article

pubs.acs.org/JCTC

# The Role of the Flexible L43-S54 Protein Loop in the CcrA Metallo-β-lactamase in Binding Structurally Dissimilar β-Lactam Antibiotics

Crystal E. Valdez, Manuel Sparta,† and Anastassia N. Alexandrova*

Department of Chemistry and Biochemistry, University of California, Los Angeles, Los Angeles, California 90095-1569, United States

**ABSTRACT:** The CcrA di-Zn β-lactamase is a bacterial enzyme capable of efficiently hydrolyzing and thus disabling a diverse set of β-lactam antibiotics. Understanding the factors that contribute to the efficiency of CcrA is essential for the design of new CcrA-resistant antibiotics and enzyme inhibitors. The efficacy of CcrA has been speculated to be partially attributable to the flexible protein loop located above the active site (L43-S54), which would mold around structurally different substrates, for snag binding. Confirmation of this hypothesis about the role of the loop has been a challenge, from both an experimental and a theoretical point of view. We employed our newly developed method that combines extensive sampling of the protein structure via discrete molecular dynamics (DMD) and quantum mechanical (QM) treatment of the active site, QM/DMD, to investigate the structural role of the L43-S54 loop in binding three different β-lactam antibiotics: imipenem, ampicillin, and cephalorodine. QM/DMD sampling was followed by high level *ab initio* calculations for the assessment of the energy contributions to loop-substrate interactions. We show that upon binding of all three antibiotic molecules, the loop comes in direct contact with the substrates and adopts distinctly different conformations depending on the bound substrate. The loop contributes to the binding affinity of CcrA to antibiotics. The primary component of the loop-substrate interaction is hydrophobic, and nonspecific, except for cephalorodine that is capable of π-stacking with W49 via one of the two competing modes.

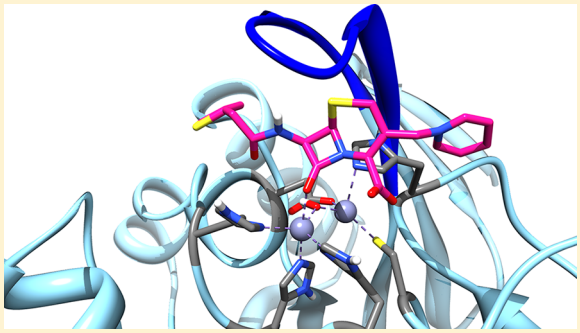

## INTRODUCTION

Antibiotic resistant bacteria are a growing worldwide concern.[1] The production of β-lactamases (EC 3.5.2.6) is the most common cause of antibiotic resistance in clinically relevant bacteria. These enzymes disable the most potent antibiotics through the hydrolysis of the β-lactam ring. β-lactamases are classified according to their amino acid sequence into four major classes (A−D). The enzymes in classes A, C, and D share a serine-based mechanism, whereas enzymes of class B depend on the presence of one or two zinc ions in the catalytic center and are known as metallo-β-lactamases.[2,3] For example, zinc-β-lactamases are responsible for antibiotic resistance in such pathogenic bacteria as *Bacteroides fragilis*,[4] *Bacillus cereus*,[5] *Stenotrophomonas meltophilia*,[6] *Pseudomonas* and *Klebsiella*,[7] *Bradyrhizobium japonicum*,[8] and *Pseudomonas aeruginosa*.[9] Among them, the di-Zn β-lactamase from *Bacteroides fragilis* (CcrA) considered in this study is one of the most versatile and dangerous,[10] due to its capability of hydrolyzing a broad spectrum of antibiotics at the diffusion-limited rate.[11]

One of the open questions regarding the functionality of CcrA is the mechanistic and structural role of residues 43−54 in its structure. These residues form a flexible hydrophobic β hairpin loop located above the active site in CcrA. It is speculated that the loop contributes to the promiscuity of CcrA and its ability to bind and hydrolyze antibiotics of diverse structures, by molding around the docked substrates. Several studies have reported on the flexibility of the β hairpin loop. Backbone heteronuclear NOE measurements indicate greater flexibility on the pico- to nanosecond time scale when compared to the entire protein.[12] Furthermore, the loop shows greater flexibility in the free CcrA compared to the inhibitor bound complexes.[13] The crystal structure of CcrA bound to a tricyclic inhibitor exhibited obvious sandwiching of the inhibitor between the active site and flexible β-hairpin loop, specifically around the GWG region.[14] Mutagenic studies of the tryptophan in the GWG region confirmed the existence of large hydrophobic contributions to the nonspecific antibiotic/loop interactions.[15] Merz and coauthors investigated the role of the loop with molecular dynamics (MD) and observed the loop's mobility and adjustment in response to the bound substrate.[16] However, purely molecular mechanical MD was unable to predict chemically meaningful binding to the metal centers, and the substrate was located over 5 Å above the active site, i.e., in a nonreactive orientation. This showed that a quantum mechanical (QM) treatment of the active site is required to produce chemically meaningful docking poses. Xu et al. investigated the Michaelis complex of moxalactam in the active site of the L1 lactamase, by means of QM/MM MD, but could not report on the role of the loop due to the short time scale of their simulation.[17] In general, elucidating the role of the loop in catalysis is a challenge, both for theory and for experimentation. Experimentally capturing the complexes of β-lactamases with their native substrates is virtually impossible, due to the high

**Received:** August 13, 2012
**Published:** October 19, 2012

  

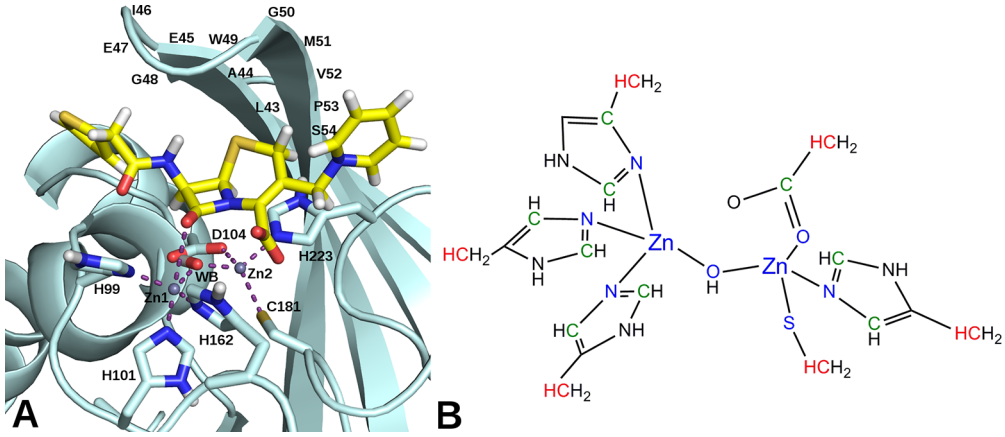


**Figure 1.** CcrA with loop, active site, and docked antibiotic cephalorodine shown. (A) In the QM/DMD simulations, the region shown in sticks constituted the QM-DMD region. (B) The green atoms show additional constraints that are imposed during the DMD simulation. To retain the chemistry determined at the QM level of theory, the red atoms are frozen during QM calculations, and the blue color marks the atoms in the QM-only domain.

catalytic efficiency of these enzymes. In theoretical modeling, quality docking that would assess the role of the loop requires both the quantum mechanical treatment of the di-Zn active site and extensive sampling of the protein structure, including the backbone and the 43−54 loop in particular.

Here, we aim at elucidating the role of the 43−54 protein loop in binding three different substrates (imipenem, ampicillin, and cephalorodine) to the active site of CcrA. Each of these molecules is a representative for a different class of $\beta$-lactam antibiotics: carbapenems, penicilins, and cephalosporins, respectively. Comparing loop interactions with a broad spectrum of substrates will elucidate the role of the loop and may contribute to the design of new generation CcrA-resistant antibiotics and inhibitors. In this study, we used our newly developed QM/DMD methodology that allows for flexible dynamic docking to metalloenzymes, with the inclusion of the quantum mechanical treatment of the metal centers. We then refine the binding energies via high level *ab initio* calculations. We elucidate the role of the flexible protein loop in binding structurally diverse substrates.

## THEORETICAL METHODS

**System Preparation.** The crystal structure of CcrA (1.85 Å resolution PDB code, 1ZNB)[18] was used as a starting point in the present investigation. Although it crystallizes as a dimer, CcrA operates as a monomer and was simulated accordingly (monomer A was used in this study). Crystallographic water molecules were removed, except for the two of them directly coordinated to the active site. The active site of CcrA contains two nonequivalent zinc ions connected by a bridging hydroxyl group (W1). Three histidine residues (H99, H101, and H162) complete the tetrahedral coordination of the first zinc (Zn1), whereas the second metal (Zn2) is coordinated by D103, C181, and H223, and a water molecule (W2) arranged in a trigonal bipyramid. This arrangement allows Zn1 to accept an additional ligand, (i.e., going from tetrahedral to trigonal bipyramid). In fact, Merz et al. demonstrated, through QM/MM calculations, that the binding mode of nitrocefin involves the interaction between the carbonyl oxygen atom of the $\beta$-lactam ring and Zn1.[19] In such a conformation, Zn1 polarizes the carbonyl group, and WB then acts as a nucleophile, attacking the carbonyl carbon atom, in the first step of hydrolysis. These ideas about substrate binding contribute to our initial guess for the CcrA-antibiotic complexes.

The loop located above the active site consists of the residues L43, A44, E45, I46, E47, G48, W49, G50, M51, V52, P53, and S54. The crystal structure did not contain residues G48 and W49, which therefore were manually built in. Upon the initial manual placement of the substrate molecules into the active site, the loop was not in contact with the substrates. Furthermore, the conformations of the side chains holding the Zn centers captured in the X-ray structure do not fully allow for the proper docking of the studied substrates in reactive orientations with respect to Zn1 and the nucleophilic hydroxyl group. In the course of QM/DMD simulations, the results of which are presented below, the substrates went deeper into the active site, and the loop was found to accommodate this binding.

The chemistry of the system dictates the choice for the QM/DMD partitioning of the system in the simulations. In QM/DMD, the system is partitioned onto three regions: the QM-only region moved by QM only, QM-DMD region that can be moved by both QM and DMD, and the rest of the system moved only by DMD (Figure 1A). The QM-DMD boundary is fluxional, and it can go around the QM-only region, or around the QM-DMD region, depending on the stage in the simulation. The QM-only region includes the two Zn centers and atoms immediately attached to them, belonging both to the substrate and to the amino acid fingers. Furthermore, additional constraints were imposed to prevent any of the residues coordinating zinc to become too distorted and lose their coordination during DMD phases. A few distances between Zn cations and certain atoms in the active site were allowed to be sampled by DMD only within ±0.01 Å from the values predicted by QM. The specific atoms are in the histidine residues, the two carbons adjacent to N coordinating Zn, the gamma carbon of the aspartate, and the beta carbon of the cysteine (Figure 1B). The QM-only region is required in order to avoid any parametrization of the classical force field for the metals, and to have instead their fully quantum mechanical description. The fuller active site contains the amino acid ligands (up to C$\alpha$ atoms) coordinating to the two Zn cations, W1, and the substrate constituted the QM-DMD region. The rest of the protein, including the 43−54 protein loop, was treated exclusively with DMD. We recently applied QM/DMD


dx.doi.org/10.1021/ct300712j | J. Chem. Theory Comput. 2013, 9, 730−737

to study a closely related system, CcrA with a smaller mimic of the $\beta$-lactam antibiotic, and obtained results for structure and reaction energies in close agreement with available theoretical and experimental data.[20]

**QM/DMD Simulations.** QM/DMD is our newly developed method that involves a QM description of the active site coupled with a discrete molecular dynamics (DMD) simulation of the entire system, including the protein backbone.[21] Briefly, DMD is a type of molecular dynamics based on solving equations of conservation of energy and momentum rather than Newtonian equations of motion.[22] It operates on a set of square well potentials, where atoms interact only as long as they are within a given distance from each other, defined by the square well. DMD is a fast and exceptionally successful method, capable of rapid sampling and simulations of protein folding and aggregation, and routinely covering time-scales on the order of tens of microseconds at least for small peptides (ca. 60 residues).[22] Density Functional Theory (DFT) was used for the QM part of simulations. The functional chosen is a pure meta-GGA functional TPSS[23] with Grimme's empirical dispersion correction[24] (TPSS-D) in conjunction with double-$\zeta$ type basis sets[25] implemented in the Turbomole software package.[26] In QM calculations, the charge of the active site is $-1$ for imipenem and cephalorodine, and $-2$ for ampicillin, and all the active sites are singlets, as predicted through our preliminary calculations.

QM/DMD simulations are performed in an iterative fashion. Each run starts from DMD operating on most of the protein, including the backbone, except for the metal centers and atoms constituting their immediate coordination sphere (QM-only region). Simulations are done using the annealing temperature profile: the temperature is initially ramped up and gradually reduced for 3500 time units (t.u.) of DMD with each time unit corresponding roughly to 50 fs. After that, the temperature is kept low for 10 000 t.u., and at that stage, data are collected. Annealing was found to help improve sampling and statistics of the resulting ensemble. The DMD-produced ensemble is clustered according to geometric similarity. In the present study, we used five clusters. Geometric centroids and lowest-energy structures are then selected from each cluster, hence a total of 10 structures are selected to represent the outcome of the current DMD phase. The QM-DMD regions are then cut out of the protein, and capped with H atoms, to satisfy all dangling valencies. The single point QM energies of the active sites are calculated. The structures are then scored, based on both the QM energy of the QM-DMD region and the DMD energy of the entire system minus the metal centers, and the smallest values of the two found in the given set of 10 structures, according to the formula:

$$\mathrm{SI}^i = n(E^i_{\mathrm{DMD}} - E^{\min}_{\mathrm{DMD}}) + (1-n)(E^i_{\mathrm{QM}} - E^{\min}_{\mathrm{QM}})$$

In this work, $n$ is set to 0.5. The structure having the smallest SI is chosen, and its active site is partially optimized quantum mechanically (for 200 steps), with the positions of the atoms bridging the QM region to the rest of the protein (C$\alpha$ atoms) being fixed. Truncated optimizations were found to be adequate to reach sufficient convergence and yet save time and increase the robustness of the algorithm. After that, the active site is uncapped and reinstalled in the protein. The QM-DMD boundary shrinks back to going around the QM-only region. The simulation continues with DMD, and at this point, the QM predicted changes in the active site have a chance to propagate to the rest of the system, in particular to the position of the protein loop of interest. QM and DMD jobs alternate to convergence in the protein structure and QM and DMD energies. The use of the fluxional QM-DMD boundary permits extensive and algorithmically simple communication between the two regions. The advantage of using the gradient following geometry optimization at the QM level instead of *ab initio* dynamics is also the gain in computational speed. The QM/DMD method is computationally affordable, while being reliable for the modeling of metalloproteins on a variety of scales from large (>10 Å), to intermediate (active site structure), to small (electronic level). Its success was recently demonstrated on such examples as $\beta$-lactamases, urease, catechol-O-methyl transferase, and rubredoxin.[20,21,27] QM/DMD recapitulated native metalloenzyme structures, predicted the structural response of the proteins to metal replacement and sequence mutations, recovered distorted proteins to the equilibrium, and generated ensembles of structures suitable for quantitative predictions of electronic properties and redox activities of metalloenzymes. In particular, QM/DMD can be used for mixed quantum-classical flexible docking. Details of the method are described elsewhere.[21]

QM/DMD simulations were run for the CcrA protein without a substrate and for the complexes with each antibiotic in duplicate. Each simulation consisted of 20 iterations alternating between DMD and QM. This corresponded to approximately 10.5 ns of dynamics for each protein. The exact timing of simulations is not extractable, because the QM part of the simulations is not done as dynamics, and the timing covered by QM may vary significantly between iterations. Finally, a long DMD-only simulation was run on the equilibrated structure, with the QM-only region fixed, in order to accumulate more statistics on the position of the loop.

**Loop/Antibiotic Interactions.** QM/DMD produced sets of structures, each resulting from the end of a single iteration, after the DMD stage. These structures (collected after the convergence within a simulation was reached) were used to calculate the interaction energies between the substrate and the protein loop, at higher levels of *ab initio* theory. Structures were chosen to be collected after the DMD phase because the protein loop of interest was not part of the QM-DMD region, and so its position was adjusted only by DMD. From each structure, we extracted the full active site with substrate and residues I46−W49 from the loop, since these were the residues that contribute to the binding of the substrate directly, in the QM/DMD generated geometries. Maintaining the geometries, we calculated the interaction energies between the active site/substrate complex and the loop using the TPSS-D3 functional with triple-$\zeta$ type basis sets in both the gas phase and in solvent using the Conductor-like Screening Model (COSMO)[28] with the dielectric constant set to 78.4 since the active site is very solvent exposed. Additionally, we performed B3LYP-D3[29] and Møller−Plesset perturbation theory calculations within the RI formalism, RI-MP2,[30] with triple-$\zeta$ type basis sets for the interaction energies. Our systems, due to their size and number of intermolecular interactions, are subject to basis superposition errors (BSSE). BSSE was accounted for using the counterpoise correction (CP) procedure as laid out by Boys and Bernardi.[31] Turbomole[26] was used for all QM calculations.

## RESULTS AND DISCUSSION

**QM/DMD Simulations.** For all studied systems, the loop was brought in close contact with the substrate almost

immediately, within 1−2 iterations. To quantify the convergence, the backbone and all heavy atom root-mean-square deviation (RMSD) of the loop as a function of the iteration number was calculated (one snapshot was used from each iteration). Because the initial PDB X-ray structure did not contain coordinates for the two residues in the flexible loop region, G48 and W49, and those residues had to be built by hand, the resultant initial structure could not be used as a reference in calculating RMSDs. Instead, the reference structure for each system was chosen via the following approach: the RMSD was calculated between all 20 structures. The structure that gave the smallest average RMSD was chosen as the reference structure. Figure 2 reports the variation of RMSD

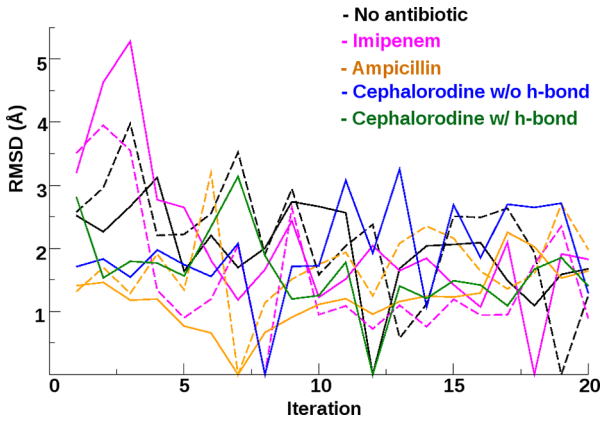


**Figure 2.** Shown are the all atom RMSDs of the active site as a function of iteration number of each antibiotic system, no antibiotic (black), imipenem (pink), ampicillin (orange), cephalospordine without constrained H-bond (blue), and cephalospordine with constrained H-bond (green). Duplicate runs are indicated by dotted lines. Each plot hits zero RMSD at the reference structure, which is different in every case (see text). The convergence of the simulations in terms of protein structure is apparent from leveling out of the plots after the 10th iteration, or earlier. Results of just one of two independent simulations are shown for each system.

with respect to this chosen structure, along the simulation. For every system, there is first a gradual reduction of RMSD, as the simulation progresses, and then stabilization of the RMSD value around the 10th iteration, indicating convergence. The relatively large fluctuations of RMSD in Figure 2 are typical for QM/DMD,[20,21,27] because the collected structures come from the ends of the DMD phases and are scored on the basis of the DMD and single point QM energies. These structures thus represent the way the DMD treats the system (on the set of square-well potentials), where there is a subtle mismatch between the QM and DMD potential energy surfaces.

QM/DMD was capable of efficiently moving protein parts in conjunction with QM description of the active site; the loop position becomes more consistent and fixed upon antibiotic binding. In Table 1, RMSD values averaged over the final 10 iterations of QM/DMD (the stage when the simulations converged) are reported for each system, in duplicate. One may see that the loop mobility varies for each antibiotic. Upon binding of ampicillin and intramolecular H-bound cephalorodine (see below), the loop mobility is indeed reduced slightly upon antibiotic binding, by ∼0.5 Å for the atoms of the loop backbone, as compared to the protein without a bound substrate. For imipenem and free cephalorodine, the RMSD values do not imply loop stabilization. The all-atom RMSD of

**Table 1. RMSD of Loop with and without Antibiotics, Averaged over the Final 10 Iterations of QM/DMD, When the Simulations Are Considered Converged, in Å**

| RMSD of loop backbone | | | | |
|---|---|---|---|---|
| no antibiotic | imipenem | ampicillin | cephalorodine | cephalorodine (H-bond) |
| 1.2 ± 0.4 | 1.2 ± 0.4 | 1.1 ± 0.4 | 1.8 ± 0.6 | 1.1 ± 0.4 |
| 1.5 ± 0.5 (1.19 ± 0.29)[a] | 1.0 ± 0.3 | 1.4 ± 0.3 | | |
| all-atom RMSD of the loop | | | | |
| 1.9 ± 0.5 | 1.7 ± 0.3 | 1.4 ± 0.4 | 2.3 ± 0.7 | 1.5 ± 0.2 |
| 1.9 ± 0.7 | 1.2 ± 0.5 | 1.9 ± 0.5 | | |

[a]Data from ref 16.

the loop calculated in the same manner is also reported in Table 1. Notice also that for cephalorodine, two different structures are reported; one of them contains an intramolecular H-bond, as will be described in detail below.

**Overall Structures of CcrA-Antibiotic Complexes Predicted by QM/DMD.** Our simulations predict that the CcrA $\beta$-lactamase indeed can tightly bind a wide spectrum of antibiotics, and the nonspecific hydrophobic interactions provided by the protein loop above the active site contribute to this versatility of CcrA. The loop visibly adjusts its structure and position in response to the presence of different substrates, and it comes into direct and tight contact with all three of them (Figure 3). The geometries of the loops adopted in each complex are distinctly different, and complementary to the bound substrates (Figure 3). At the atomic level, the only specific interaction found in the complexes is the one between the W49 side chain of the loop and the aromatic ring in the cephalorodine antibiotic. Specifics of this contact that helps substrate binding are explicated below. All other interactions between the loop and the substrates are hydrophobic and nonspecific. Our results support the earlier proposal[13−15] that the loop molds around substrates of different shapes, upon substrate binding.

The structural parameters of the active site of CcrA not bound to any substrate were found to be close to those predicted by purely quantum mechanical calculations on small model complexes.[32] For the bound active site−substrate complexes, our simulations predict binding that is consistent with quantum mechanical calculations on the active site model, but that is much tighter as compared to the structures produced by purely force field based molecular dynamics (Table 2 and Figure 4).[14] The carbonyl oxygen atom is located within ca. 2.5 Å from Zn1 and the carbonyl carbon atoms, within ca. 3.5 Å from the nucleophilic OH. These structural characteristics of the protein−substrate complexes are remarkably consistent within each QM/DMD ensemble, and also across the set of studied antibiotics. The average bond lengths of the lactam ring carbonyl and Zn1 of the three antibiotic systems are listed in Table 1. One important observation should be made about cephalorodine. In its complex with CcrA, two competitive configurations were identified. In one of them, the molecule formed an intramolecular H-bond between H1 and O3 (see Figure 3), and in the other one the molecule was extended. These structures are listed separately in Tables 1 and 2; a detailed discussion is presented in the next section. All structures of the protein−antibiotic complexes are available upon request. They can be used as starting points for mechanistic studies.


dx.doi.org/10.1021/ct300712j | J. Chem. Theory Comput. 2013, 9, 730−737

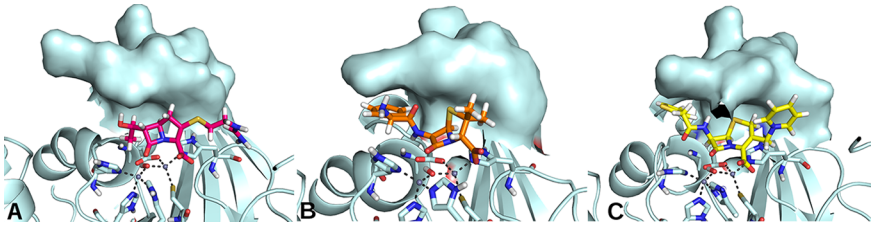


**Figure 3.** Representative snapshots from QM/DMD simulations for imipenem (A), ampicillin (B), and cephalorodine (C) bound to CcrA showing the distinctly different conformations of the residues in the hydrophobic $\beta$-hairpin loop adopted in response to binding different substrates. The loop in space filling mode is shown above the active site.

**Table 2. Important Antibiotic/Active Site Interatomic Distances Averaged over 20 Structures Extracted from the Converged States of Two Independent QM/MD Simulations for Each System, in Å[a]**

| | imipenem | ampicillin | cephalorodine | cephalorodine (H-bond) |
|---|---|---|---|---|
| Zn1–O1 | 2.9 ± 0.4 | 2.7 ± 0.5 | 3.3 ± 0.3 | 2.6 ± 0.2 |
| | 2.6 ± 0.1 (5.93 ± 0.40)[b] | 4.7 ± 0.3 | | |
| C2–$O_{WB}$ | 3.1 ± 0.3 | 3.0 ± 0.3 | 2.8 ± 0.2 | 2.4 ± 0.3 |
| | 3.0 ± 0.1 (5.55 ± 0.32)[b] | 3.8 ± 0.3 | | |
| Zn2–O2 | 5.4 ± 1.2 | 4.4 ± 1.6 | 9.8 ± 0.3 | 9.1 ± 0.3 |
| | 6.3 ± 1.2 | 3.6 ± 0.9 | | |
| Zn2–O3 | 6.1 ± 1.3 | 5.5 ± 0.8 | 10.9 ± 0.3 | 10.1 ± 0.4 |
| | 7.6 ± 1.3 | 5.7 ± 0.7 | | |

[a]Atoms are labeled as in Figure 4. [b]Data from ref 16.

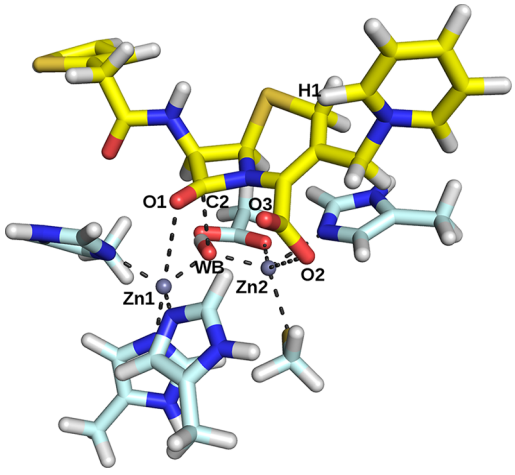


**Figure 4.** Illustrating important interatomic distances listed in Table 1 in the antibiotic/active site complexes (shown here with cephalorodine).

**Position and Mobility of the Loop in the CcrA Alone, and in Complexes with Three Antibiotics.** QM/DMD simulations done on the empty proteins indicate a significant mobility of the loop. In Figure 5, snapshots coming from QM/DMD simulations are overlaid. The snapshot shown in green is the initial structure, which is shown just for reference, but really should not be considered. The rest of the ensemble is not well-clustered and samples a large conformational space.

When antibiotics molecules bind to the active site, the preferred conformations and the mobility of the loop change. Different and unique loop conformations are predicted for each antibiotic uptaken by CcrA. For ampicillin (Figure 5B, and Table 1), the loop adopts a rigid conformation. The QM/DMD ensemble is tightly clustered. Clearly the loop rigidity is induced by the bound antibiotic. However, when imipenem is bound, the loop is not as well structured, and multiple conformations of the loop can be found, showing its flexibility (Figure 5C). The tail of the molecule extending toward the loop is smaller, hydrophilic, and charged. Therefore, hydrophobic contacts with the loop are largely avoided by this part of the bound substrate. However, the loop molds around the rest of the substrate, as seen in Figure 3. The residue of the loop closest to imipenem is W49, but even it does not form any efficient interactions. Recent experiments with BlaB metallo-$\beta$-lactamase showed that both of these antibiotics are efficiently hydrolyzed by it, at a rate comparable with that of CcrA, and the smaller tail of imipenem did not have any effect on binding or turnover rate of the enzyme.[33] In agreement with this finding, the position of the substrate with respect to the Zn centers and the nucleophilic bridging water is consistent with those characteristic of other studied antibiotics (Table 2).

QM/DMD simulations yielded a more complicated story of the cephalorodine binding (Figure 5D–F). In this antibiotic, there appears to be a weak intramolecular H-bond between the carboxylic oxygen and the pyridine group hydrogen (H1–O3, in Figure 4). This H-bond is not recognized by the force field implemented in DMD, because of the atypical H-bond donor involved. However, QM calculations predict this H-bond for the substrate bound to the active site. Whether it is QM or DMD that should be trusted is questionable, because despite the higher accuracy, QM calculations did not include the residues of the loop. As a result, our initial QM/DMD simulation on this complex failed to converge and showed swapping between two different conformations predicted by QM and DMD. At the same time, the pyridine group of the substrate adopted two different conformations corresponding to perpendicular and parallel $\pi$-stacking interactions with the loop residue W49 (Figure 5D,F).

To further investigate this issue, we introduced an additional constraint on the distance between the carboxylic oxygen and the pyridine group C donating the H-bond in the DMD part of the simulation. Sampling of this distance was allowed within ±0.1 Å from the value predicted by QM calculations. With this constraint, the simulation yielded a stable intermolecular H-bond, and an exclusively parallel $\pi$-stacking interaction with W49 (Figure 5E,F). Interestingly, constrained and unconstrained simulations yield similar QM energies, the differences within 4.5 kcal/mol, and converge to a similar DMD energy range. From this we infer that perhaps all three conformations of cephalorodine bound to CcrA may exist: with intramolecular H-bond and parallel $\pi$-stack with W49, without H-bond and with parallel $\pi$-stack, and without H-bond and with perpendicular $\pi$-stack. This versatility should contribute

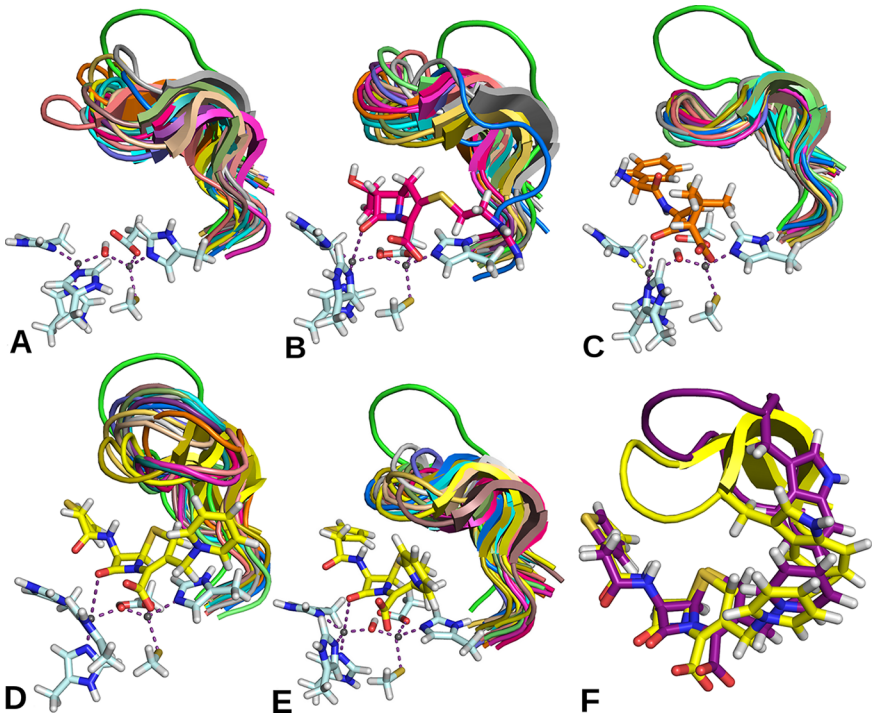


**Figure 5.** Overlaid images of the snapshots from the QM/DMD simulation illustrating the mobility and adjustment of the $\beta$-hairpin loop: (A) no antibiotic is bound, (B) imipenem, (C) ampicillin, (D) cephalorodine (simulation without a constraint), (E) cephalorodine (simulation with a constraint) bound to CcrA. (F) Two possible $\pi$-stacking orientations between W49 and the cephalorodine molecule, parallel and perpendicular, are seen in the simulation with D. The larger mobility of the loop when no antibiotic is present at the active site can be seen. The snapshot in green is the initial conformation of the loop in each simulation.

favorably to the binding process through configurational entropy and facilitate the hydrolysis of this molecule by CcrA. This result is somewhat paradoxical, since cephalorodine is the bulkiest of the studied antibiotic molecules. Our result agrees with an earlier report suggesting the interaction of cephalorodine with W49.[14]

In order to analyze the interactions of the loop with antibiotics, we assessed the mobility of the loop residues in each complex (Figure 6). It can be seen that, for each amino acid, the average all atom RMSD is the highest when no antibiotic is bound, in agreement with the reduced loop mobility upon locking onto the substrate. Also, naturally, the residues in the middle of the loop are more mobile than the ones nears its ends. As mentioned above, the loop, when ampicillin is bound, adopts a slightly more rigid conformation, and this is shown in the individual residue RMSDs. On the other hand, when imipenem is bound, the loop is more flexible and can adapt multiple conformations, especially the hydrophobic residues, W49−V52, closest to its hydrophilic tail. For cephalorodine, the simulation without the H-bond enforced yielded the two conformations of W49, while the one without the H-bonding did not. Comparing the RMSD of W49 of these two simulations, the RMSD for cephalorodine with the H-bond is definitely higher than the one without, by ∼0.5 Å. Overall, individual amino acid RMSDs differ relatively little between different antibiotics. These results are consistent with the bonding between the loop and the substrates being nonspecific in each case.

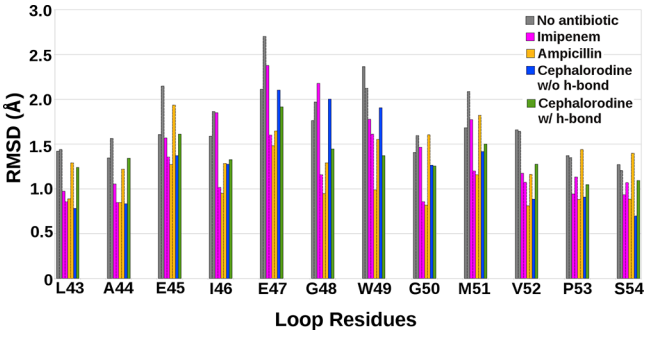


**Figure 6.** The average all atom RMSDs for each residue in the loop shows greater flexibility for the more solvent exposed, polar residues such as E28 and W49. The dotted line columns correspond to the duplicate simulation for the no antibiotic, imipenem and ampicillin systems. The reference structure used for calculating the RMSDs are the same ones used to calculate the RMSDs of the loop during the QM/DMD simulations.

**Loop-Substrate Interaction Energies.** The interaction between the $\beta$-hairpin loop and antibiotic was evaluated by comparing binding energies. Structures used to evaluate those interactions resulted from the DMD stages of QM/DMD simulations, when the position of the loop was the most realistic. The systems used for the binding energies calculations include the loop, antibiotic, and active site chopped as it is during the QM stage of QM/DMD. Of the 12 residues in the loop (L43−S54) only residues I46−W49 were used in these calculations, to decrease the system size. Those residues were found to have the closest contact with the substrates and hence are expected to contribute the most to the substrate binding energies. Loop-substrate interaction energies were calculated as the difference between the energy of the entire complex and the sum of the energies of the loop and the joint antibiotic-active site part. Table 3 lists all the BSSE-corrected binding energies


dx.doi.org/10.1021/ct300712j | J. Chem. Theory Comput. 2013, 9, 730−737

Table 3. Binding Energies of All Loop/Antibiotics Systems at the DFT Level, in kcal/mol

| B.E. | imipenem | ampicillin | cephalorodine | cephalorodine (H-bond) |
|---|---|---|---|---|
| TPSS-D3/def2-TZVPP | 48.6 ± 5.0 (51.1 ± 3.7) | 16.7 ± 5.4 (16.3 ± 6.3) | 56.6 ± 7.9 | 56.6 ± 4.7 |
| TPSS/def2-TZVPP (no dispersion) | 35.0 ± 3.7 (36.4 ± 4.8) | −6.7 ± 5.6 (−1.4 ± 4.8) | 37.7 ± 5.2 | 33.9 ± 4.4 |
| TPSS/def2-TZVPP (no dispersion) + CP | 34.4 ± 3.7 (35.5 ± 4.8) | −7.1 ± 5.6 (−1.8 ± 4.8) | 36.9 ± 5.2 | 32.6 ± 4.4 |
| TPSS-D3/def2-TZVPP + solvent | 5.9 ± 2.2 (4.0 ± 1.7) | 4.3 ± 3.8 (3.2 ± 4.1) | 0.9 ± 3.5 | 7.3 ± 2.6 |
| TPSS-D3/def2-TZVPP + solvent + CP | 5.2 ± 2.1 (3.2 ± 1.7) | 3.9 ± 3.8 (2.9 ± 4.1) | −0.4 ± 3.5 | 6.1 ± 2.6 |
| B3LYP-D3/def2-TZVP + solvent + CP | 5.8 ± 2.1 (−7.8 ± 2.1) | 4.0 ± 4.3 (−6.9 ± 4.5) | 0.0 ± 3.6 | 7.4 ± 3.2 |
| MP2/def2-TZVPP | 35.9 ± 7.0 (48.5 ± 9.6) | 20.6 ± 5.4 (20.4 ± 8.1) | 45.3 ± 11.2 | 51.8 ± 7.8 |

with respective antibiotics. In this work, positive binding energies correspond to favorable and stabilizing interactions. As apparent from the values presented in Table 3, inclusion of solvation dramatically lowers the estimated loop-antibiotic affinities and therefore is essential for the assessment. On the other hand, the large basis sets used in the final energy calculations limit the BSSE to ca. 1 kcal/mol.

As one would expect from the nature of the interaction between the antibiotics and the loop, the major component to the binding energy is the dispersion interactions. The contributions of dispersion to the binding energies are also included in all DFT calculations.

For all antibiotics, these values are similar, small, and positive, indicating weakly attractive interactions. Our results suggest that, even though the loop above the active site plays a major role in binding structurally dissimilar substrates, the loop-substrate interaction energies are not different enough to be a defining factor in the efficiency of hydrolysis of these molecules by CcrA.

## CONCLUSIONS

The CcrA $\beta$-lactamase enzyme is capable of hydrolyzing a large class of structurally different antibiotics. The presence of the flexible loop above the active site was long thought to contribute to the substrate binding and enzyme promiscuity. Through this work we were able to see that loop/antibiotic interactions play a role in stabilizing the antibiotic for hydrolysis. The work features our new method, QM/DMD, capable of performing efficient quality QM/MM docking to flexible active sites of metalloproteins. All antibiotics exhibit snag binding to the flexible loop, and this greatly reduces its mobility. The positions of the loop are substrate-specific, indicating the loop adjustment and molding around bound substrates, in agreement with earlier proposals. For imipenem and ampicillin, no specific interactions between the loop and the substrates can be found, and the interaction is essentially hydrophobic. For cephalorodine, the aromatic ring of the substrate can $\pi$-stack with W49 of the loop and orient itself in parallel or perpendicular orientation with respect to this residue. In all cases, the primary loop-substrate interaction component is dispersion. This work contributes to mechanistic studies of CcrA and potentially can help the design of inhibitors and more potent, CcrA-resistant antibiotics. Structures of all CcrA-antibiotic complexes are available upon request.

## AUTHOR INFORMATION

### Corresponding Author

*E-mail: ana@chem.ucla.edu.

### Present Address

[†]Max Planck Institute for Chemical Energy Conversion, Stiftstr. 34-36, 45470 Mülheim an der Ruhr, Germany.

### Notes

The authors declare no competing financial interest.

## ACKNOWLEDGMENTS

This work was supported by the DARPA Young Faculty Award N66001-11-1-4138, and the NSF Graduate Fellowship #2011115747 (CEV).

## REFERENCES

(1) Wang, Z.; Fast, W.; Valentine, A. M.; Benkovic, S. J. *Curr. Opin. Chem. Biol.* **1999**, *3* (5), 614−622.
(2) Ambler, R. P. *Phil. Trans. R. Soc. London, Ser. B* **1980**, *289*, 321−331.
(3) Bush, K.; Jacoby, G.; Medeiros, A. A. *Antimicrob. Agents Chemother.* **1995**, *39*, 1211−1233.
(4) Cuchural, G. J.; Malamy, M. H.; Tally, F. P. *Antimicrob. Agents Chemother.* **1986**, *30*, 645−648.
(5) Sabath, L. D.; Abraham, E. P. *Biochem. J.* **1966**, *98*, 11c−13c.
(6) Ullah, J. H.; Walsh, T. R.; Taylor, I. A.; Emery, D. C.; Verma, C. S.; Gamblin, S. J.; Spencer, J. *J. Mol. Biol.* **1998**, *284*, 125−136.
(7) Senda, K.; Arakawa, Y.; Ichiyama, S.; Nakashima, K.; Ito, H.; Ohsuka, S.; Shimokata, K.; Kato, N.; Ohta, M. *J. Clin. Microbiol.* **1996**, *34*, 2909−2913.
(8) Docquier, J.-D.; Benvenuti, M.; Calderone, V.; Stoczko, M.; Menciassi, N.; Rossolini, G. M.; Mangani, S. *Antimicrob. Agents Chemother.* **2010**, *54*, 4343−4351.
(9) Leiros, H. K.; Bora, P. S.; Bandsdal, B. O.; Edvardsen, K. S.; Spencer, J.; Walsh, T. R.; Samuelsen, O. *Antimicrob. Agents Chemother.* **2012**, *56*, 4341−4353.
(10) Felici, A.; Amicosante, G.; Oratore, A.; Strom, R.; Ledent, P.; Joris, B.; Fanuel, L.; Frère, J. M. *Biochem. J.* **1993**, *291*, 151−155.
(11) Carfi, A.; Duée, E.; Paul-Soto, R.; Galleni, M.; Frére, J. M.; Dideberg, O. *Acta Crystallogr., Sect. D* **1998**, *54*, 47−57.
(12) Scrofani, S. D. B.; Chung, J.; Huntley, J. J. A.; Benkovic, S. J.; Wright, P. E.; Dyson, H. J. *Biochemistry* **1999**, *38*, 14507−14514.
(13) Fitzgerald, P. M. D.; Wu, J. K.; Toney, J. H. *Biochemistry* **1998**, *37*, 6791−6800.
(14) Payne, D. J.; Hueso-Rodrieguez, J. A.; Boyd, H.; Conca, N. O.; Janson, C. A.; Gilpin, M.; Bateson, J. H.; Cheever, C.; Niconovich, N. L.; Pearson, S.; Rittenhouse, S.; Tew, D.; Diez, E.; Perez, P.; de la Fuente, J.; Rees, M.; Rivera-Sagredo, A. *Antimicrob. Agents Chemother.* **2002**, *46*, 1880−1886.
(15) Huntly, J. J. A.; Fast, W.; Benkovic, S. J.; Wright, P. E.; Dyson, J. *Protein Sci.* **2003**, *12*, 1368−1375.
(16) Suárez, D.; Días, N.; Merz, K. M. *J. Comput. Chem.* **2002**, *23*, 1587−1600.
(17) Xu, D.; Cui, Q.; Guo, H. *J. Phys. Chem. A* **2007**, *111*, 5630−5636.
(18) Concha, N. O.; Rasmussen, B. A.; Bush, K.; Herzberg, O. *Structure* **1996**, *4*, 823−836.
(19) Park, H.; Brothers, E. N.; Merz, K. M., Jr. *J. Am. Chem. Soc.* **2005**, *127*, 4232−4241.
(20) Valdez, C. E.; Alexandrova, A. N. *J. Phys. Chem. B.* **2012**, *116*, 10649−19656.
(21) Sparta, M.; Ding, F.; Shirvanyants, D.; Dokholyan, N. V.; Alexandrova, A. N. *Biophys. J.* **2012**, *103*, 767−776.

(22) (a) Dokholyan, N. V.; Buldyrev, S. V.; Stanley, H. E.; Shakhnovich, E. I. *Fold. Des.* **1998**, *3*, 577−588. (b) Ding, F.; Guo, W.; Dokholyan, N. V.; Shakhnovich, E. I.; Shea, J. E. *J. Mol. Biol.* **2005**, *350*, 1035−1050. (c) Dokholyan, N. V. *Curr. Opin. Struct. Biol.* **2006**, *16*, 79−85. (d) Ding, F.; Tsao, D.; Nie, H.; Dokholyan, N. V. *Structure* **2008**, *16*, 1010−1018.
(23) Tao, J.; Perdew, J. P.; Staroverov, V. N.; Scuseria, G. E. *Phys. Rev. Lett.* **2003**, *91*, 146401−146401.
(24) Grimme, S. *J. Comput. Chem.* **2006**, *27*, 1787−1799.
(25) Weigend, F.; Ahlrichs, R. *Phys. Chem. Chem. Phys.* **2005**, *7* (18), 3297−3305.
(26) *Turbomole*, v6.3; University of Karlsruhe: Karlsruhe, Germany, 2011. Available from http://www.turbomole.com.
(27) Sparta, M.; Alexandrova, A. N. *PLoS ONE* **2012**, in press.
(28) Klamt, A.; Schüürmann, G. J. *Chem. Soc. Perkin Trans.2* **1993**, *5*, 799−805.
(29) (a) Becke, A. D. *J. Chem. Phys.* **1993**, *98*, 5648−5652. (b) Grimme, S.; Antony, J.; Ehrlich, S.; Krieg, H. *J. Chem. Phys.* **2010**, *132*, 154104−15419.
(30) (a) Head-Gordon, M.; Pople, J. A.; Frisch, M. J. *Chem. Phys. Lett.* **1988**, *153*, 503−506. (b) Frisch, M. J.; Head-Gordon, M.; Pople, J. A. *Chem. Phys. Lett.* **1990**, *166*, 275−280. (c) Frisch, M. J.; Head-Gordon, M.; Pople, J. A. *Chem. Phys. Lett.* **1990**, *166*, 281−289. (d) Weigend, F.; Häser, M. *Theor. Chem. Acc.* **1997**, *97*, 331−340.
(31) Boys, S. F.; Bernardi, F. *Mol. Phys.* **1970**, *19*, 553−566.
(32) Días, N.; Suárez, D.; Merz, K. M. *J. Am. Chem. Soc.* **2000**, *122*, 4197−4208.
(33) Vessillier, S.; Docquier, J.; Rival, S.; Frere, J.; Galleni, M.; Amicosante, G.; Rossolini, G.; Franceschini, N. *Antimicrob. Agents Chemother.* **2002**, *46* (6), 1921−1927.